The International Journal of Advanced Manufacturing Technology (2018) 97:13–24
https://doi.org/10.1007/s00170-018-1886-0

ORIGINAL ARTICLE

Effects of process parameters on force reduction and temperature variation during ultrasonic assisted incremental sheet forming process

Yangyang Long[1] · Yanle Li[2,3] · Jie Sun[2,3] · Igor Ille[1] · Jianfeng Li[2,3] · Jens Twiefel[1]

Received: 24 August 2017 / Accepted: 13 March 2018 / Published online: 26 March 2018

Abstract
The incremental sheet forming (ISF) is an innovative dieless forming process featured with high formability and short lead time which is suitable for rapid prototyping and small volume production. The integration of ultrasonic (US) vibration into the ISF process can significantly reduce the forming force and bring other benefits. In this work, the impacts of process parameters including the sheet material, US power, feeding speed, and tool diameter, on force reduction and temperature increment were studied. The force reduction contains two components—the stress superposition-induced force reduction and acoustic softening-induced force reduction. The stress superposition-induced force reduction was analyzed by finite element simulation while the total force reduction was detected by experiments since currently, the unknown mechanism of the acoustic softening cannot be modeled. The temperature increment was measured by a high-speed infrared camera. The results show that the force reduction can go up to 56.58% and the temperature increment can be as high as 24.55 °C. In general, the material with a higher yield stress results in a higher force reduction and a higher temperature increment. A higher US power or a lower feeding speed can significantly enhance the force reduction and the interface temperature increment. The tool with a smaller diameter has a comparable effect as a larger tool, but a larger vibration amplitude is required.

Keywords Ultrasonic vibration · Incremental sheet forming · Force reduction · Interface temperature

1 Introduction

Flexible sheet forming technologies play a significant role to advance the manufacturing level and the capacity of the aerospace industry, especially for complex thin-wall metallic components featured with high-performance, low-batch, and short delivery time. Incremental sheet forming (ISF) process is known as a potential technology ideal for rapid prototyping and small batch productions. In an ISF process, a hemispherical-ended forming tool incrementally deforms a flat metal sheet into the designed 3D shape. The moving trajectory was achieved through computer numerical controlled (CNC) system. By using this technique, no specialized tooling is required and sheet parts can be formed directly from computer-aided design (CAD) data. The concept of ISF was proposed by Leszak [1] in 1967 and was proven to be feasible by Kitazawa et al. [2] in forming rotational symmetric parts with aluminum. The capability study of using an ordinary CNC milling machine instead of a special designed machine-tool apparatus was later performed by Jeswiet [3]. The first commercial machine dedicated for ISF was produced by AMINO Corporation [4].

The research emphases of ISF during the past decades are geometric accuracy, surface finish, and thickness thinning. Ambrogio et al. [5] statistically analyzed the effects of process parameters including tool diameter, step down, wall angle, final product depth, and the sheet thickness, on geometric accuracy of the formed truncated cone. It was suggested that the geometric error measured at the corner was largely influenced by the sheet thickness and the total part depth. Different kinds of strategies have been adopted by researchers to improve the geometric accuracy under clamping condition. Allwood et al. [6]

✉ Yanle Li
yanle.li@sdu.edu.cn

[1] Institute of Dynamics and Vibration Research, Leibniz Universität Hannover, Appelstr. 11, 30167 Hannover, Germany

[2] School of Mechanical Engineering and Key Laboratory of High Efficiency and Clean Mechanical Manufacture, Shandong University, No. 17923 Jingshi Rd, Jinan 250061, China

[3] National Demonstration Center for Experimental Mechanical Engineering Education, Shandong University, Jinan 250061, China

demonstrated an approach to reduce geometric error by introducing partial cut-outs to weaken the local sheet blank. Lu et al. [7] demonstrated a significant improvement on the geometrical accuracy of the formed component wall by adopting a model predictive control method. The surface finish quality is regarded as another weak point in ISF. Durante et al. [8] (2010) described a model for evaluating the roughness in terms of both amplitude and spacing associated with three parameters: the slope angle, the step-down size, and the tool radius. Later, Hamilton et al. [9] investigated the influences of tool feed rates and spindle rotation at high speeds during forming on the non-contact side roughness. Also, a model for the orange peel prediction in SPIF was established, which provided some guidelines for the improvement of external surface quality.

In recent years, various hybrid incremental forming strategies have been proposed with the aim to satisfy industrial requirements. Mohammadi [10] have developed a laser-assisted incremental forming process (LASPIF) by adding a dynamic heating system. It was concluded from the experimental results that this strategy can provide with a better geometric accuracy, lower forming forces, and improved formability. Malhotra et al. [11] developed a platform which enables double-sided incremental forming (DSIF) to reduce the significant amount of bending at the edges of the component. Also, electric-assisted incremental sheet forming has been investigated by Liu et al. [12] to improve the formability of the "hard-to-form" materials such as titanium alloy. However, rough surface of the formed part and sever tool wear are the main challenges of this promising forming strategy. Electromagnetic incremental forming (EMIF) has been carried out by Cui et al. [13] to form large-scale sheet but it was concluded that the thickness thinning in EMIF is significantly decreased.

An emerging approach for solving the mentioned issues is the ultrasonic (US)-assisted ISF. By the integration of US into the ISF process, many benefits can be brought in as can be seen from other US-assisted metal forming processes such as press forming, deep drawing, upsetting, wire drawing, and tube spinning, etc. [14]. In general, US brings two effects including volume effect and surface effect.

The volume effect is also termed as the Blaha effect or Acoustoplastic effect (APE) since it was discovered by Blaha and Langenecker [15]. When an 800 kHz vibration was superimposed on a tensile test of a single zinc crystal, they found big flow stress reduction (~ 40%) during the plastic deformation stage. Two hypotheses were then proposed to explain the underlying mechanism. One is stress superposition (SS) raised by Nevill and Brotzen [16] who argued that a simple superposition of an oscillatory stress to a steady stress could explain the APE effect. In 1959, Blaha and Langenecker [17] reported the other hypothesis—acoustic softening (AS): in addition to the stress superposition, the defects within crystals, especially dislocations, absorbed the acoustic energy and were activated from their pinned positions. Over the past decades, arguments about the two hypotheses never stopped.

Until the recent 10 years, the acoustic softening hypothesis was proven by applying piezo force sensors. With such a method, Daud et al. [18, 19] separated the APE effect into AS and SS during US vibration superimposed tensile and compression tests. Similar conclusions were obtained and validated by Aziz [20] and Yao et al. [21]. As a result, it is confirmed that the APE effect contains two parts, as illustrated in Fig. 1. Part I also contains friction reduction which is very difficult to be separated from AS. In this work, the force reduction caused by both AS and friction reduction is simply stated as AS effect.

The surface effect brought by US is on friction. When a contact of surfaces exists, a friction reduction always occurs in accompany with the APE effect. As indicated by Storck et al. [22], the reduction is only an average force reduction within a macroscopic time-scale. In other words, the friction itself is not reduced while in reality, more friction is introduced due to the back and forth relative motion of the two contact surfaces.

The benefits of the US-assisted ISF process has been rarely studied. Vahdati et al. [23] and Amini et al. [24] investigated the US effect on AA1050-O sheet forming. They claimed that the forming force could be reduced for 23.5 and 26.3% during the vertical and horizontal movement, respectively. In addition, it has been shown that the formability of the sheets and the surface quality were enhanced while the spring-back coefficient decreased by adding US. Qi et al. [25] investigated the effect of ultrasonic vibration on micro-channeling through both numerical and experimental approaches. The impacts of process parameters on the forming process, however, have not yet been studied.

The aim of this work is to fill this gap. The impacts of the process parameters including sheet material, US power, tool diameter, and feeding speed, on both volume effect and surface effect, were investigated. The volume effect is studied by the force reduction caused by APE as well as the SS and AS components. The surface effect is investigated by analyzing the temperature increment of the sheets since more friction is introduced by US vibration. In Sect. 2, the simulation and the

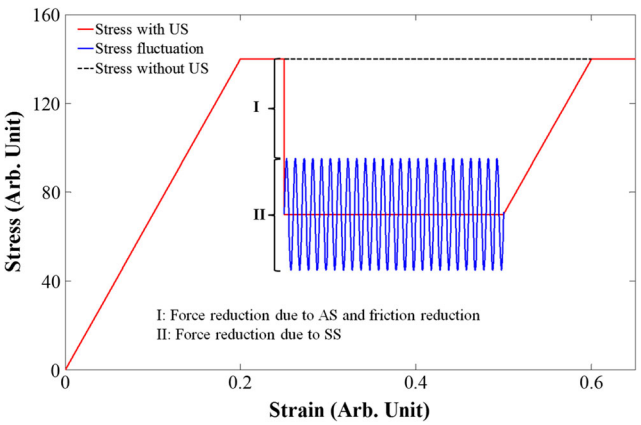

Fig. 1 Illumination of the two components of APE

experimental setups are described. The results of the impacts of process parameters on force reduction and enhanced temperature are provided and discussed in Sect. 3.

2 Methods

As discussed in the introduction, the volume effect—APE—has two components which are SS and AS. The SS can be simulated with finite element method (FEM) and the whole APE-induced force reduction can be experimentally detected. Due to the complexity of the AS, the fundamental mechanisms have not yet been fully understood. As a result, the effect of AS is currently unable to be modeled. In this case, the AS-induced force reduction is obtained by subtracting the SS-induced component from the whole APE-induced force reduction. The surface effect—friction—is investigated by the measurements of the temperature changes at the tool/sheet interface. A point-sheet forming (1D sheet forming) process is used for the investigation so that the influence of horizontal movement-induced friction on APE and temperature increments can be minimized.

2.1 Establishment of the FE model

In the present work, FE simulations were performed by LS-DYNA to investigate the stress-superposition (SS)-induced force reduction during the point sheet forming process. In these models, forming tools were defined as rigid bodies and only the displacements along the axial direction were allowed. Specifically, the ultrasonic vibration of the forming tool was defined as an additional displacement to the normal movement as follows:

$$Z = vt + Asin(2\pi f) \tag{1}$$

where Z is the axial displacement, v is the feeding speed, A is the vibration amplitude, and f is the vibration frequency which can be set independently. The metal sheets with a diameter of 140 mm were modeled with the shell element type 163 and were initially meshed at the size of 1.6 mm to improve the computing efficiency. To ensure the simulation accuracy, the elements at the deformation zone at the center area were further refined to the size of 0.57 mm. In terms of the boundary conditions in the FE model of the forming process, nodes within a range of 15 mm to the edges of the circular sheet are constrained in all degrees of freedom to represent the clapping constraint. The thickness of the sheets was 1.0 mm which is the same as in the experiments. The material properties are listed in Table 1. Swift's isotropic strain hardening laws were used for representing the plastic behavior of the sheet materials. To investigate the effects of material type, tool size, and vibration amplitude on the forming process, 16 cases with different parameter settings were simulated as listed in Table 2.

2.2 Experimental setup

To investigate the impacts of the processing parameters on the total force reduction and the temperature change during the forming process, two US-assisted point sheet forming test benches were established. In addition to the parameters which are simulated as in Table 2, the feeding speed was also varied to study its influence.

2.2.1 Ultrasonic system

The ultrasonic system consists of a transducer, a sonotrode (the forming tool), and a driving system. The transducer as shown in Fig. 2 is a "sandwich" type piezo-electric transducer with a six-piezo element stack, which can efficiently convert electric energy into mechanical vibration. It was designed at IDS with an eigenfrequency of ~ 21 kHz and a high quality factor of ~ 800.

In order to analyze the influence of the tool diameter on the forming process, two sonotrodes were designed. As shown in Fig. 2, the tool tips have a half-sphere shape with different diameters—10 and 20 mm. The forming tool is made of tool steel AISI M2 that is commonly used for ISF. The AISI M2 steel has an elastic modulus of ~ 200 GPa and a compressive yield stress of 3.25 GPa. The forming tool was connected to the transducer to constitute the actuator for sheet forming. With a frequency response measurement, the eigenfrequencies of the actuator for 10 mm and 20 mm tool are ~ 21.3 and ~ 21 kHz, respectively. The shift of the eigenfrequency from the designed value is due to the machining and the hardening processes.

The piezo-actuator was driven by a digital phase controller DPC 500/100k and an audio amplifier QSC RMX 4050HD. The digital phase controller is an in-house developed controller while the amplifier was received from QSC AG. The phase controller generates a sinusoid

Table 1 The mechanical properties of the sheet materials

Material	Elastic modulus (GPa)	Yield stress (MPa)	Ultimate stress (MPa)	Poisson ratio	Plastic hardening law
AA1050-H14	70	100	135	0.33	$\delta = 145.47\varepsilon^{0.05}$
AA5052-H34	76	172	235	0.33	$\delta = 117\left(1 + \frac{\varepsilon}{0.0045}\right)^{0.22}$

The plastic hardening law for AA1050 and AA5052 is obtained from Noh et al. (2016) and Woo et al. (2017), respectively

Table 2 FE simulation cases with parameter settings

Simulation case No.	Material	Tool diameter (D/mm)	Vibration amplitude (A/μm)
1	AA1050	10	0
2			12
3			15
4			18
5		20	0
6			6
7			9
8			12
9	AA5052	10	0
10			12
11			15
12			18
13		20	0
14			6
15			9
16			12

voltage signal to the amplifier and the amplified voltage is used to drive the actuator. The driving voltage and current of the actuator were monitored by a voltage probe and a current probe, respectively. The monitored values were sent back to the phase controller for phase and current feedback control. The principle of the closed controlling loop is shown in Fig. 3. C_p is the capacitance of the transducer; PSD is the phase sensitive demodulation; DDS is the direct digit synthesizer; and κ is the gain of the amplifier. The controlling frequency of the phase controller is 500 Hz which enables the actuator to keep on resonance and constant current during the forming process.

2.2.2 Force detection

The actuator was fixed to a linear stage, as shown in Fig. 4. The linear stage is CKK 20-145 and driven by a MSK 030C motor, purchased from Rexroth Bosch Group and Lenze Vertrieb GmbH, respectively. The fixture of the plate is also shown in Fig. 4. The whole fixture was placed on a force transducer, C6A purchased from Hottinger Baldwin Messtechnik GmbH. After the

Fig. 2 The transducer and two sonotrodes

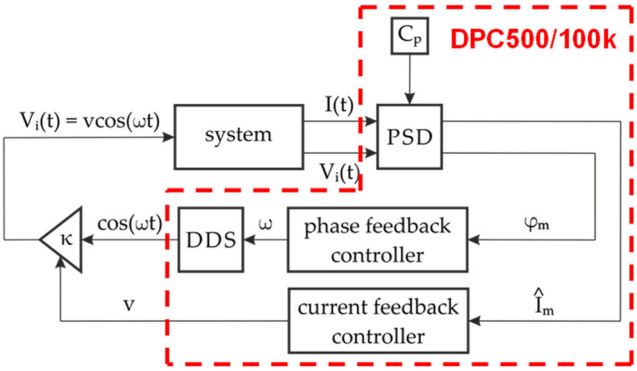

Fig. 3 The principle of the closed controlling loop

amplification, the force signal was acquired by a NI DAQ system and then read by a Labview program. The sampling rate in the experiments was 1000 p/s which is high enough for the force detection.

2.2.3 High-speed temperature detection

To capture the temperature changes during the sheet forming process, a high-speed infrared camera was vertically installed underneath the sheet fixture, as shown in Fig. 5. The camera used is a long wave length infrared camera SC7300L from Flir System Inc. The MCT detector consists of 320 × 256 pixels and the pixel size is 30 × 30 μm. With a full window size, the video recording rate is up to 231 fps. A L0306 lens with a focal length of 12 mm and an aperture of 2.0 was used. The focal plane with a large depth of field was adjusted to the position of the sheet so that the whole forming process can be accurately detected. Together with the lens, the system possesses a resolution of 294 × 294 μm/pixel.

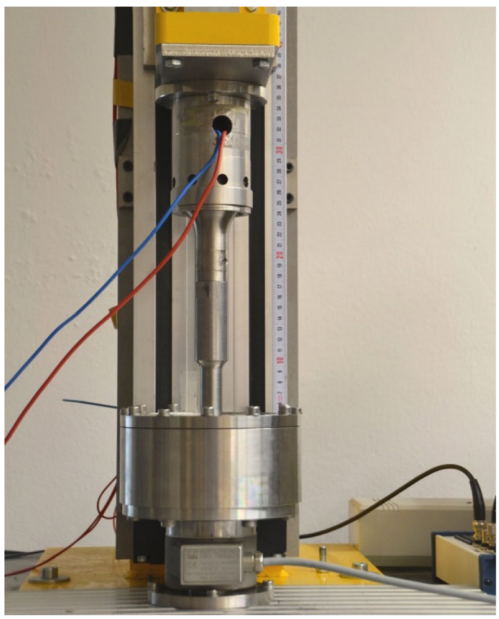

Fig. 4 The linear stage and the force detection setup

Fig. 5 Temperature detection with the high-speed infrared camera

2.2.4 Sheet materials

Two different aluminum materials—AA1050-H14 and AA5052-H34—were used for studying the impact of sheet materials. The elastic modulus, the yield, and ultimate stress of the materials are already shown in Table 1. All the sheets have a thickness of 1 mm and were cut into a circular shape with Ø140 mm by laser. Since the surface of aluminum sheet has a very high reflectivity, which is not good for infrared temperature measurements, one side of the sheets was spray-coated with a thin graphite layer. Since the graphite layer is much thinner than the aluminum sheet and the heat conductivity (168 W/(m × K) at room temperature) is close to that of aluminum, the influence of the graphite layer is negligible. The emissivity of the graphite layer was chosen to be 0.95.

2.2.5 Vibration amplitude

The vibration amplitudes of the forming tools were detected by an out of plane laser-vibrometer OFV 552 from Polytec Inc. The measurements were conducted under free load and with different power inputs. The zero-to-peak amplitudes of the tool tip point along with different US power inputs for the two forming tools are plotted in Fig. 6a, b, respectively.

Due to the big step change of the sonotrode, the 10-mm forming tool can reach a much higher amplitude. The 10-mm tool composed actuator was driven by an US power of 15~30 W. The corresponding amplitude to 30 W at the tip point was 18 μm. The 20 mm forming tool in the experiment was driven by an US power of 30~60 W. The maximum vibration amplitude of the tool tip point within this power range is 12 μm. The amplitudes at the other points of the half-sphere were also measured. At a point with a radius of 9.3 mm to the central tip point, the vibration amplitude (11.9 μm) was still quite close to the tip point. This means that the vibration of the half-sphere was quite even.

As mentioned before, the US system was controlled by both phase feedback and current feedback loops. This ensured that the vibration amplitude of the forming tool kept constant during the forming process even under dynamic loadings. A maximum power of ~ 50 and ~ 80 W was needed to keep the vibration of the 10-mm tool and 20-mm tool at their largest amplitudes during the tests, respectively. This means that the US vibration was more efficiently applied compared to those in other studies.

3 Results and discussion

3.1 State of stress and strain with SS-induced force reduction

In order to investigate and quantify the local deformation behavior during the point-forming process, four distinct

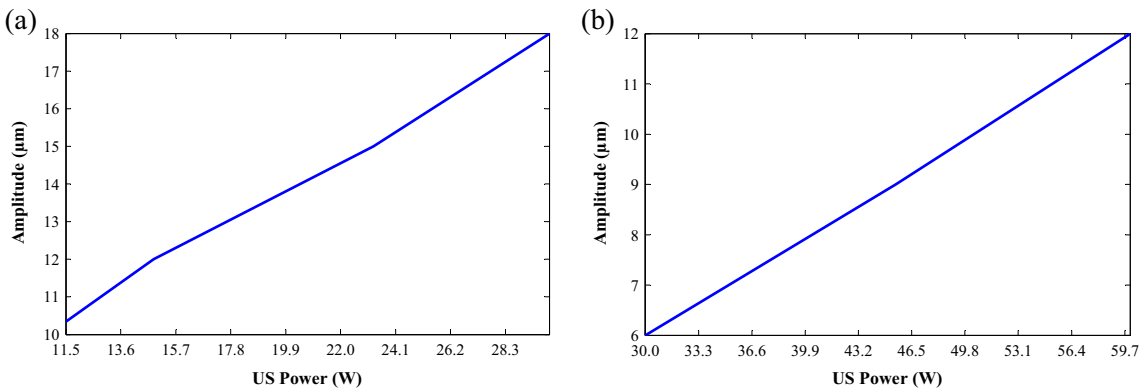

Fig. 6 Vibration amplitudes of tool tip vs. driving current for the forming tool with a diameter of **a** 10 mm and **b** 20 mm

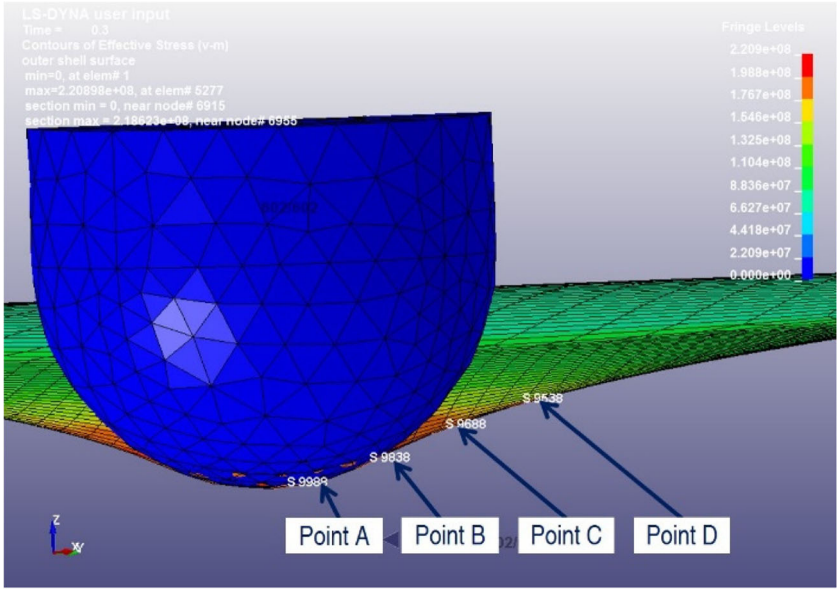

Fig. 7 FE model of the point-forming process with four selected critical elements marked

elements (A to D from the center to the outer as shown in Fig. 7) along the inclined wall were selected. Furthermore, the averaged effective plastic strain and stress for each element were investigated.

Figure 8a shows the effective strain evolution of points A to D during the forming process for AA1050 sheets. In this forming case, the tool size was 10 mm and the vibration amplitude was 18 μm. It was shown that the effective plastic strains for all the points are increasing continuously with the forming depth, which reflects the inherent mechanics of incremental sheet forming. However, the effective plastic strain at points C and D is relatively small (less than 0.15) compared with values at point A (0.8 maximum). This is explained by the fact that these two points are located away from the center zone and no substantial plastic deformation is expected. It can also be noticed that the other two points (A and B) present more severe plastic deformation, which correspond to the current contact zone. Similarly, the effective stress of the four selected points is presented in Fig. 8b. It was noticed that, at the initial stage, the effective stresses (von-Mises) were oscillating under US vibration. This may be due to that the tool was hammering the material and the sheet was experiencing high frequent instantaneous load. However, at the later stage, the material was deformed larger than the yield condition and the tool was always contacting with the sheet.

The SS effect of vibration amplitude on strain behavior at the center (point A) of the sheet is also investigated. As shown in Fig. 9a, the effective plastic strain increases as the increase of the vibration amplitude. Additionally, an initial sharp increase can be observed for effective strains under US vibration. At the initial stage, the material has not reached the yield condition, higher amplitude leads to larger magnitude of the instantaneous press of the tool in a vibration cycle. This results in a relatively larger deformation of the plate material per unit area. Similarly, the SS effect of vibration amplitude on stress behavior at the center (point A) of the sheet is compared in Fig. 9b. It was observed that, at the same forming depth, the effective stress was reduced due to the SS effect by the US vibration and the stress reduction is proportional to the value of the vibration amplitude.

3.2 Impact of process parameters on force reduction

With the integration of US vibration, a significant force reduction can be obtained. An example is shown in Fig. 10 where an AA1050 sheet was pressed by the 20-mm tool. The difference of the forming forces between the simulated value and the

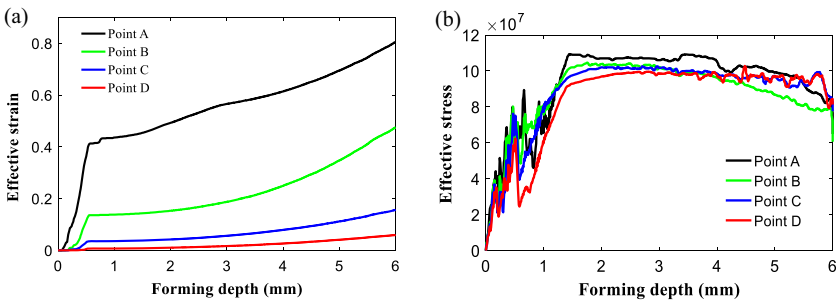

Fig. 8 **a** Effective strain. **b** Effective stress at different points for AA1050 material (D = 10 mm, A = 18 μm)

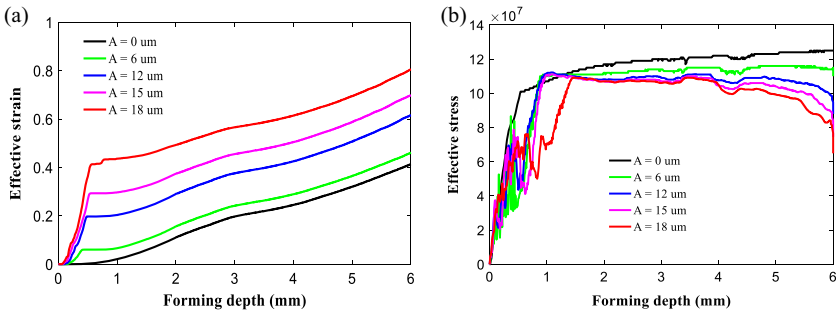

Fig. 9 **a** Effective strain and **b** effective stress for point A with different amplitudes AA1050 material with 10 mm forming tool

experimental value is within an acceptable range, considering only a standard power law constitutive model was used for the sheet material. Since only the stress superposition-induced force reduction was simulated in the FE model, a distinguish difference between the simulated force and the experimental force with 12 μm vibration can be observed. In the following results, the SS-induced force reduction is obtained by FE simulations and the AS was calculated by subtracting SS from APE obtained by experiments.

3.2.1 Effect of material

The 20-mm forming tool was first used for the force reduction analysis. The driving US power was set to the maximum value so that the largest amplitude 12 μm can be reached. The vertical feeding speed of the forming tool was kept at 0.1 mm/s and the maximum feeding distance was 5.0 mm for both materials. The corresponding force reduction for each material is shown in Fig. 11.

From the figure, it can be seen that the forming force is greatly influenced by the sheet material. It seems that the force reduction depends on the yield stress of the material. For the soft material AA1050, the total force reduction was only 37.07% while the value went up to 56.58% for AA5052 with a much larger yield stress. As discussed before, the APE consists of SS and AS. The SS-induced force reduction has been obtained by the FE simulation, and the AS was calculated by subtracting SS from APE. It is obvious in the figure that both components of APE are significantly influenced by the material. For a harder material, a larger stress superposition is required since the vibration amplitude stays the same. As a result, the SS effect is more profound for AA5052. The AS needs to be analyzed based on Langenecker's theory. In general, a hard aluminum alloy has more defects than a soft aluminum alloy. According to Langenecker (1962), the US energy is only absorbed by defects. When more defects were pushed by acoustic waves from their pinned positions, the hard material received a larger force reduction. In an extreme situation where all defects can be activated by acoustic waves, the force required for the plastic deformation will be zero and the yield stress can represent the force reduction. On the other hand, the high acoustic softening-induced force reduction for AA5052 indicates that the acoustic waves are preferred to be absorbed by defects.

3.2.2 Effect of US power

Different US powers were applied to different sheets for studying the effect of US power on the force reduction. The sheets were formed with the 20-mm tool at a feeding speed of 0.1 mm/s and a feeding distance of 5.0 mm. The force reductions for using different US power inputs are shown in Fig. 12. Since it is more straightforward to explain vibration by amplitude, different amplitudes are used here instead using US

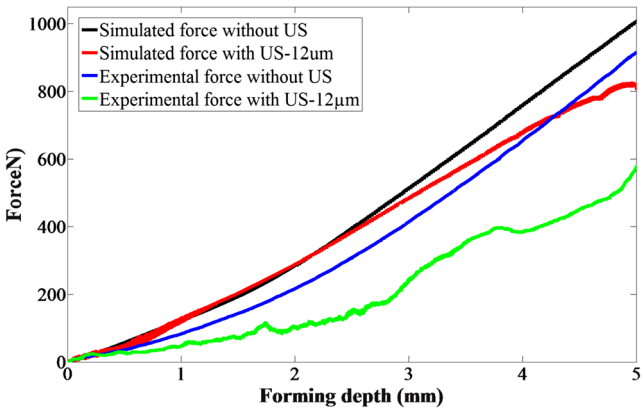

Fig. 10 The forming force during the forming process with 20-mm tool and AA1050

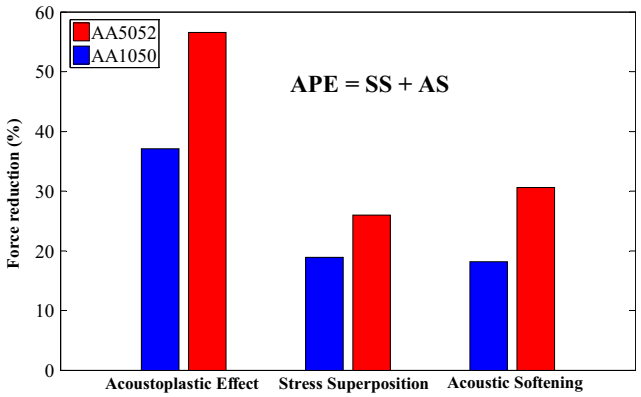

Fig. 11 Impact of materials on force reduction with US—12- and 20-mm tool

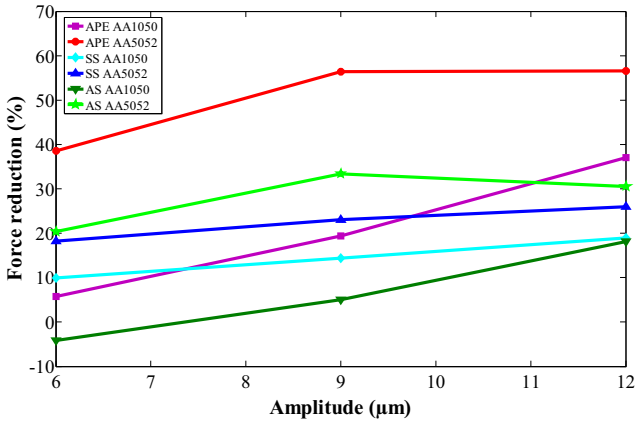

Fig. 12 Impact of US power on force reduction for **a** AA1050 and **b** AA5052 with 20-mm tool

power. The corresponding US power to these amplitudes can be found in Fig. 6.

With no doubt, the APE effect increases as the vibration amplitude increases since more SS and AS shall be imposed to the material. From Fig. 12, it can be seen that the influence of the amplitude is significant for both material. The only exception is the AS effect on AA5052 for which a slight decrease took place when the amplitude exceeded 9 μm. This might be due to the inconsistence between the simulation and the experimental results. But in general, all the effects have the same incremental tendency along with the increase of the amplitude. This is in agreement with the literature in which the APE effect was shown to be dependent on the vibration amplitude.

3.2.3 Effect of tool diameter

Two forming tools were designed for analyzing the influence of tool diameter on the forming process. It has been shown that the 20-mm forming tool can greatly reduce the forming force. The 10-mm forming tool was then installed, and the results are compared to the 20-mm forming tool, as shown in Fig. 13. All experiments were conducted with a feeding speed of 0.1 mm/s.

For the 10-mm forming tool, similar influences of the material and the vibration amplitude can be observed. The AA5052 with a greater yield stress received the largest total force reduction. Both SS and AS effects become more profound when comparing Fig. 13a, b. When the amplitude increased, the same incremental tendency as 20-mm tool can be observed. When the amplitudes for both tools are 12 μm, the total force reduction of 20-mm tool on both materials is much larger than that of 10-mm tool. As the vibration amplitude of 10-mm tool increased, the difference to the 20-mm tool with 12-μm amplitude got smaller and smaller. This is understandable since more surface areas of the tool and the sheets got into contact for the 20-mm tool and more US energy can be transferred to the sheets. Concluding, the tool with a smaller diameter has a comparable effect as a larger tool, but larger vibration amplitude is required.

3.2.4 Effect of feeding speed

In addition to the above parameters, the feeding speed was varied to form the two different sheets for studying the influence of the feeding speed on force reduction. The processes were performed with 12-μm amplitude and the 20-mm tool. The force reductions for a feeding distance of 5.0 mm are shown in Table 3.

It can be clearly seen that a higher feeding speed led to a lower force reduction rate. This can be explained by the transfer of the US energy. With a higher feeding speed, less US energy per time unit was transferred into the sheets. As a result, the APE effect to the sheet forming decreased and a larger force was required. For AA1050, the force reduction significantly decreased and this could indicate a bad coupling between the tool and the AA1050 sheets. In the real sheet forming process, a compromise between the feeding speed and the forming force needs to be made.

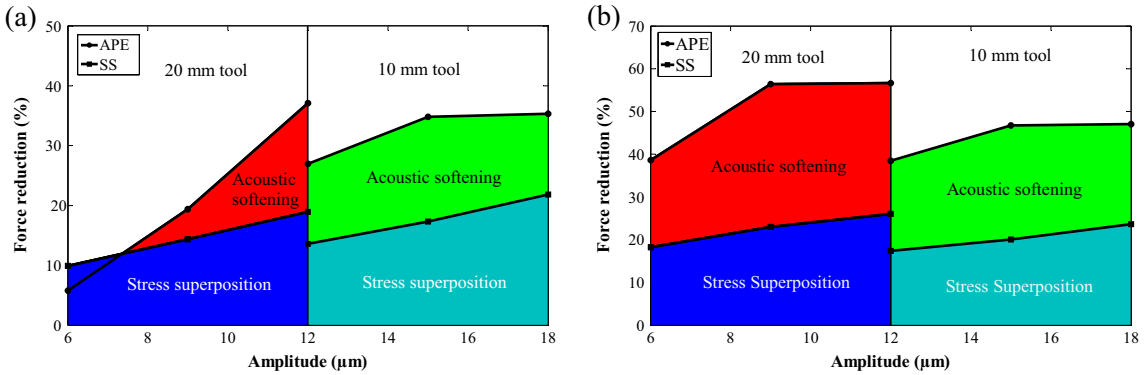

Fig. 13 Impact of tool diameter on force reduction for **a** AA1050 and **b** AA5052

Table 3 Force reduction with different feeding speeds

Material	Force reduction (%)	
	0.1 mm/s	0.3 mm/s
AA1050-H14	37.07	5.79
AA5052-H34	56.58	41.39

3.3 Impact of process parameters on temperature increments

The surface effect brought by US vibration was investigated by analyzing the temperature increment of the central part of the sheets. Due to the vibration, additional friction cycles were added at the tool/sheet interface. And this led to a higher temperature at the tool/sheet interface. The temperature changes were directly monitored by a high-speed infrared camera installed at the bottom of the sheet fixture. The detected temperature at the bottom surface of the sheets can also reflect the interface temperature changes.

An example where an AA5052 sheet was pressed by the 20 mm tool with a feeding speed of 0.1 mm/s and a distance of 5.0 mm is shown in Fig. 14. The first forming process as shown in a, c, e ran without US while the second process as shown in b, d, f ran with a vibration amplitude of 12 μm. It can be clearly seen that the US vibration greatly enhanced the temperature inside the sheets, especially the central region where the tool directly contacted the sheets.

The temperature changes at the tip point throughout the forming process are illustrated in Fig. 15. The noise in Fig. 15a comes from the quantization of the camera and the zoom of the scale. Without an US input, the maximum change was only 1.09 °C; while the value dramatically increased to 17.96 °C when the 12-μm US vibraion was applied. Figure 15a shows a two-step temperature increment. The first increase was associated with the initial elastic deformation during which the deformation rate

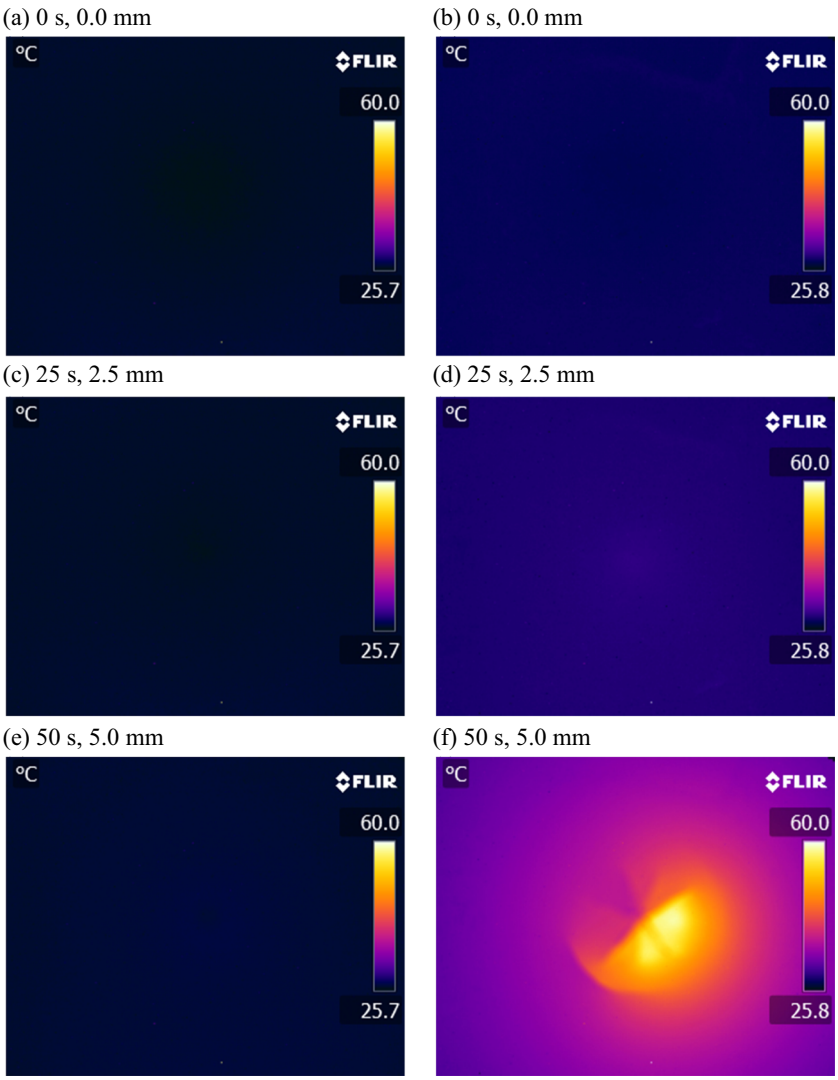

Fig. 14 Thermal images during the forming process of AA5052 with 20-mm tool for **a**, **c, e** without US and **b**, **d**, **f** with US-12 μm

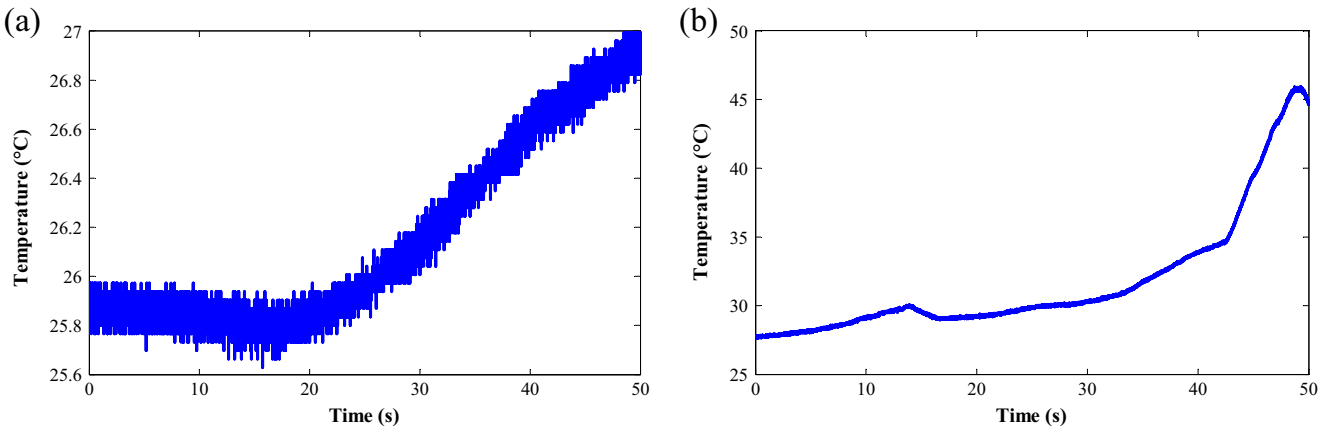

Fig. 15 The temperature changes at the tip point for **a** without US and **b** with US-12 μm

was big and the friction between the tool and the sheets increased. After this period, more area between the tool and the sheets got contacted and some friction-induced heat was absorbed by the tool. As the normal stress became larger and the deformation got into plastic stage, the friction-induced heat increased again until the process ended. The temperature increment for the US-assisted process is similar. This is attributed to the vibration-induced friction depending on the normal stress and the coupling conditions at the moment. In the first ~ 30 s, the stress was small and a micro-hammer effect could exist at the tool/sheet interface, which means that the tool was not always contacting the sheet during a single vibration period. These led to a slow increase of the temperature. As the deformation became larger, the stress got larger and the micro-hammer effect got weakened or even vanished. As a result, the temperature increased much faster during the latter stage. The increased heat brought by US vibration also helps the softening of the material and release part of the residual stress inside the sheets.

When the forming process finished, the temperature distributions at the central line are displayed in Fig. 16. Due to the slow temperature change and the high heat conductivity of aluminum, the central part of the curve shows a flat feature. The exception took place at the tip point where the temperature was smaller than the surrounding points. This can be caused by the heat transfer from the sheet to the tool tip. With US vibration, the friction between the tool and the sheets generated large amounts of heat, leading to the peak at the central region. Since the central region was deformed from a circle to a "star" shape as in Fig. 14f, an asymmetric feature appeared at the central line.

3.3.1 Effect of material

Similar experiments have been conducted on AA1050 sheets under the same settings. The results also indicate a dramatic increment in temperature by adding US vibration. The results are compared in Table 4. The AA1050 sheets exhibited similar temperature increment as AA5052.

Two main reasons caused the similar temperature increments. First, the normal stresses during the two processes were similar. Even though AA5052 has a larger yield stress, it has been decreased to the same level as AA1050 by US vibration at the same deformation rate. Second, a micro-hammer effect between the tool and AA5052 sheets resulted

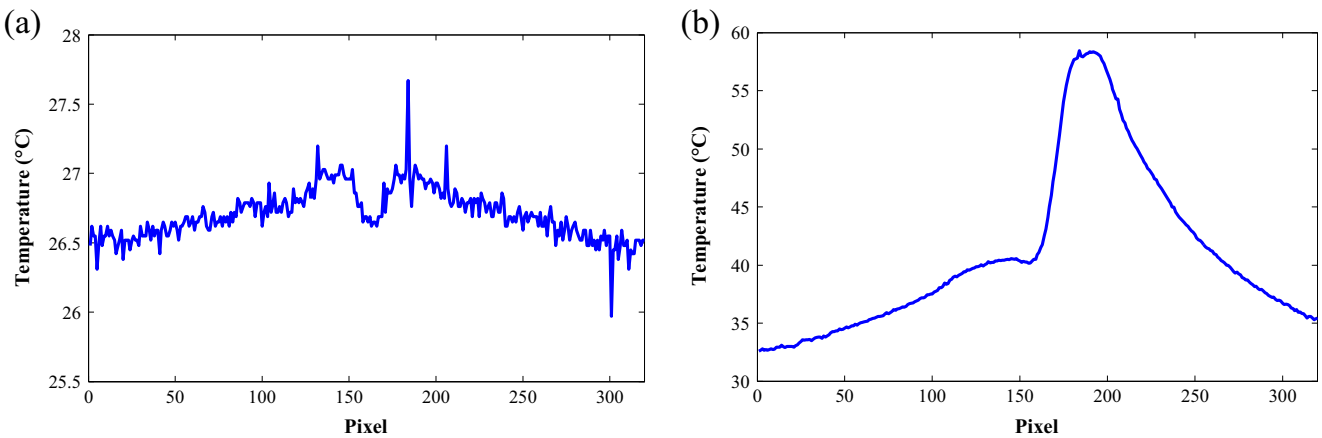

Fig. 16 Temperature distributions at the central line for **a** without US and **b** with 30 W US

Table 4 Impact of material on temperature increment

Material	Temperature increment (°C)	
	0 μm	12 μm
AA1050-H14	1.78	18.01
AA5052-H34	1.09	17.96

in less friction; on the other hand, the internal friction of AA5052 was higher since more defects were moving during the US imposition period. The higher internal friction compensated the loss of external friction.

3.3.2 Effect of US power

To test the impact of US power on the temperature increment, different US powers (vibration amplitude) were applied to the two different sheets. The sheets were formed with 20-mm tool at a feeding speed of 0.1 mm/s and a feeding distance of 5.0 mm. The results are shown in Table 5.

The big difference on the temperature increments indicates the significant impact of US power. When a higher vibration amplitude was added, a larger force reduction was generated. However, the relative motion routes became much longer. If the micro-hammer effect is not considered, the relative motion routes for each period shall be increased for two times. This leads to a significant enhancement of the temperature increment.

3.3.3 Effect of tool diameter

The impact of tool diameter on the temperature increment is shown in Table 6. When the amplitude for both tools was 12 μm, the temperature increments for 10-mm tool were obviously smaller than that for 20-mm tool. This is due to the larger normal force for 20 mm tool and the larger contact area with the sheets. The difference became smaller as the vibration amplitude of the 10-mm tool increased since more friction was generated. Specifically for the 10-mm tool, it shows a different impact on the temperature increments. Since the friction was constrained in a much smaller contact interface, the heat conductivity became a significant factor. AA1050 has a much larger heat conductivity (227 W/m-K) than AA5052 (138 W/m-K) but a similar heat capacity (0.900 J/g-°C for AA1050, 0.880 J/g-°C for AA5052). The large heat conductivity effectively transferred the heat to the other part of the AA1050 sheets so that it showed a much smaller temperature increment compared to AA5052.

Table 5 Impact of vibration amplitude on temperature increment

Material	Temperature increment (°C)	
	6 μm	12 μm
AA1050-H14	11.59	18.01
AA5052-H34	5.78	17.96

Table 6 Impact of tool diameter on temperature increment

Material	Temperature increment (°C)		
	10 mm (12 μm)	10 mm (18 μm)	20 mm (12 μm)
AA1050-H14	4.13	11.83	18.01
AA5052-H34	13.53	24.55	17.96

3.3.4 Effect of feeding speed

When the feeding speed increased, the forming process got shorter. Since the vibration frequency was fixed, the vibration-induced friction cycles decreased. On the other hand, when US vibration was not added, the deformation caused temperature increment would increase as the time was shorter. However, since the vibration-induced heat was much larger, the total temperature increment was assumed to decrease. The assumption was validated by the experiment performed with the 20-mm tool and a feeding distance of 5.0 mm, as shown in Table 7.

4 Conclusions

Based on our simulation and experimental results, the following conclusions can be made.

- The forming force can be greatly reduced by the application of US vibration during the forming process. The SS-nduced force reduction was simulated with finite element method (FEM) and the whole APE-induced force reduction was detected experimentally in the presented work.
- The sheets with a higher yield stress received more SS and absorbed more US energy which led to a higher force reduction. A higher US power and a smaller feeding speed can significantly enhance the APE effect as well as the SS and AS components. A smaller tool had an equivalent influence on the force reduction but needs a higher vibration amplitude.

Table 7 Impact of feeding speed on temperature increment

Material	Temperature increment (°C)	
	0.1 mm/s	0.3 mm/s
AA1050-H14	18.01	13.09
AA5052-H34	17.96	14.55

- The integration of US vibration dramatically increased the temperature of the sheets. A higher US power and a smaller feeding speed led to a further enhancement of the temperature increment. For the 20-mm tool, the temperature increment of AA1050 was larger than that of AA5052 at 6-μm vibration and equal to that of AA5052 at 12-μm vibration. For the 10-mm tool, AA5052 had a much larger temperature increment. The increased temperature helps the sheet deformation and the release of the residual stress.

The micro-hammer behavior during the forming process as well as its influence will be studied in the near future.

Acknowledgements The authors would like to thank the preparatory visit funding from Sino-German Center for Research Promotion (GZ1381). Dr. Yanle Li is also funded by National Natural Science Foundation of China (51605258), China Postdoctoral Science Foundation funded project (2016M592180), and Postdoctoral innovation project of Shandong Province (201701011).

References

1. Leszak E (1967) Apparatus and process for incremental dieless forming. USA Patent 3342051A
2. Kitazawa K, Wakabayashi A, Murata K, Yaejima K (1996) Metal-flow phenomena in computerized numerically controlled incremental stretch-expanding of aluminum sheets, vol 46. vol 2. Keikinzoku Tokyo
3. Jeswiet J (2001) Incremental single point forming. Trans North Am Manuf Res Inst SME 29:75–79
4. Amino M, Mizoguchi M, Terauchi Y, Maki T (2014) Current status of "Dieless" Amino's incremental forming. Procedia Engineering 81(0):54–62
5. Ambrogio G, Cozza V, Filice L, Micari F (2007) An analytical model for improving precision in single point incremental forming. J Mater Process Technol 191(1–3):92–95
6. Allwood JM, Braun D, Music O (2010) The effect of partially cut-out blanks on geometric accuracy in incremental sheet forming. J Mater Process Technol 210(11):1501–1510
7. Lu H, Kearney M, Li Y, Liu S, Daniel WJT, Meehan PA (2016) Model predictive control of incremental sheet forming for geometric accuracy improvement. Int J Adv Manuf Technol 82(9–12): 1781–1794
8. Durante M, Formisano A, Langella A (2010) Comparison between analytical and experimental roughness values of components created by incremental forming. J Mater Process Technol 210(14):1934–1941
9. Hamilton K, Jeswiet J (2010) Single point incremental forming at high feed rates and rotational speeds: surface and structural consequences. CIRP Ann Manuf Technol 59(1):311–314
10. Mohammadi A, Vanhove H, Van Bael A, Duflou JR (2016) Towards accuracy improvement in single point incremental forming of shallow parts formed under laser assisted conditions. Int J Mater Form 9(3):339–351
11. Malhotra R, Cao J, Beltran M, Xu D, Magargee J, Kiridena V, Xia ZC (2012) Accumulative-DSIF strategy for enhancing process capabilities in incremental forming. CIRP Ann Manuf Technol 61(1): 251–254
12. Liu R, Lu B, Xu D, Chen J, Chen F, Ou H, Long H (2016) Development of novel tools for electricity-assisted incremental sheet forming of titanium alloy. Int J Adv Manuf Technol 85(5): 1137–1144
13. Cui XH, Mo JH, Li JJ, Zhao J, Zhu Y, Huang L, Li ZW, Zhong K (2014) Electromagnetic incremental forming (EMIF): a novel aluminum alloy sheet and tube forming technology. J Mater Process Technol 214(2):409–427
14. Rasoli MA, Abdullah A, Farzin M, Tehrani AF, Taherizadeh A (2012) Influence of ultrasonic vibrations on tube spinning process. J Mater Process Technol 212(6):1443–1452
15. Blaha F, Langenecker B (1955) Dehnung von Zink-Kristallen unter Ultraschalleinwirkung. Naturwissenschaften 45(20):556–556 **(in German)**
16. Nevill GE, Brotzen FR (1957) The effect of vibrations on the static yield strength of a low-carbon steel. Proc Am Soc Test Mater 57: 751–758
17. Blaha F, Langenecker B (1959) Ultrasonic investigation of the plasticity of metal crystals. Acta Metall 7(2):93–100
18. Daud Y, Lucas M, Huang Z (2007) Modelling the effects of superimposed ultrasonic vibrations on tension and compression tests of aluminium. J Mater Process Technol 186(1–3):179–190
19. Daud Y, Lucas M, Huang Z (2006) Superimposed ultrasonic oscillations in compression tests of aluminium. Ultrasonics 44(SUPPL): e511–e515
20. Aziz SA, Lucas M (2012) Characterising the acoustoplastic effect in an ultrasonically assisted metal forming process. IOP Conf Ser Mater Sci Eng 42:012017. https://doi.org/10.1088/1757-899X/42/1/012017
21. Yao Z, Kim GY, Faidley L, Zou Q, Mei D, Chen Z (2012) Effects of superimposed high-frequency vibration on deformation of aluminum in micro/meso-scale upsetting. J Mater Process Technol 212(3):640–646
22. Storck H, Littmann W, Wallaschek J, Mracek M (2002) The effect of friction reduction in presence of ultrasonic vibrations and its relevance to travelling wave ultrasonic motors. Ultrasonics 40(1–8):379–383
23. Vahdati M, Mahdavinejad R, Amini S (2015) Investigation of the ultrasonic vibration effect in incremental sheet metal forming process. Proceedings of the Institution of mechanical engineers, Part B J Eng Manuf
24. Amini S, Hosseinpour Gollo A, Paktinat H (2016) An investigation of conventional and ultrasonic-assisted incremental forming of annealed AA1050 sheet. Int J Adv Manuf Technol:1–10
25. Qi H, Wen DH, Lu CD, Li G (2016) Numerical and experimental study on ultrasonic vibration-assisted micro-channelling of glasses using an abrasive slurry jet. Int J Mech Sci 110:94–107

Publisher's Note